

Supporting Information

Spectral Tuning in Halorhodopsin: The Chloride Pump Photoreceptor

Rhitankar Pal, Sivakumar Sekharan^{*} and Victor S. Batista^{*}

Department of Chemistry, Yale University, P.O. Box 208107, New Haven, CT 06520-8107

Table of Contents (total pages 16)

- I. System setup.
- II. Sequence alignment between bacteriorhodopsin and halorhodopsin.
- III. Comparison of the X-Ray and QM/MM optimized distances between key residues in the active site.
- IV. Structural rearrangements due to H95 mutants.
- V. Structural rearrangements due to Q105, T111 and T203 mutants.
- VI. Structural rearrangements due to R108 mutants.
- VII. The QM/MM optimized structural models of shR with potassium (K^+) or with chloride (Cl^-) at the CB2 site.
- VIII. Comparison of the QM/MM optimized diamond shaped and pentagonal water cluster in the active site of shR.
- IX. Correlation between the total number of intermolecular hydrogen bonding networks in the active site and frontier molecular orbital analysis of the electronic transition responsible for wavelength of maximal absorption in shR.
- X. Distances of key hydrogen bonding networks in the active site.
- XI. SORCI+Q(6,6) calculated vertical excitation energies in gas phase and protein environment.
- XII. Geometrical parameters of the all-*trans*-retinyl chromophore in the QM/MM optimized wildtype and mutant shR models.
- XIII. References for the Supporting Information.
- XIV. Complete references from the manuscript.

I. System setup

Halorhodopsin of *H. salinarum* (shR) is composed of 274 amino acids (aa's), of which the X-ray structure (1E12)¹ contains only residues from 24 to 262. Residues 1 to 23 and 263 to 274 have not been resolved and thus the QM/MM model contains 239 aa's. In the QM/MM model, 12 sites are negatively charged (D25, E90, E100, D128, D130, D141, D182, E194, D197, E219, D238, E257) and 11 sites are positively charged (R24, R52, R55, R58, R60, R103, R108, R161, R200, R251, R258). The protonation states of all titratable residues ($\text{pH}=7$) are assigned using PROPKA calculations implemented in the Schrodinger's Maestro v.9.3 software package² and visual inspection. The system contains a total of 96 water molecules. Three water molecules (w2023, 2081, 2082) are present near the chromophore and mediate the hydrogen-bonding network in the active site. A potassium ion was found to be situated underneath helix B and located at $\sim 19 \text{ \AA}$ to the SB. However, further X-ray refinement and mutation of site T203 (T203V, PDB code: 2JAG)³ yielded the L1-intermediate and also a second chloride binding-site (CB2), where CB2 was shown to be occupying the site originally assigned for the potassium ion in the 1E12 X-ray structure. Although the present QM/MM study was based on the 1E12 X-ray structure, we have modelled shR with both K^+ and Cl^- ions underneath helix B and the resulting structural differences are shown in section V. As a result, the overall charge of the QM/MM system varies from neutral ($0e$, due to the presence of K^+ at CB2) to anionic ($-2e$, due to the presence of Cl^- at CB2) and the results reported in this work correspond to the QM/MM model with Cl^- at CB2. To minimize the structural changes and to preserve the natural shape of the protein, the full structure was relaxed via a three-step optimization procedure. First, the system was relaxed at the MM level, followed by relaxation at the mechanical-embedding (ME) level and finally, the whole protein was relaxed without any constraints at the EE level of theory. An overlay of the QM/MM optimized geometry with the X-ray structure (Fig. S1) shows that the overall shape of the protein was preserved during the optimization steps.

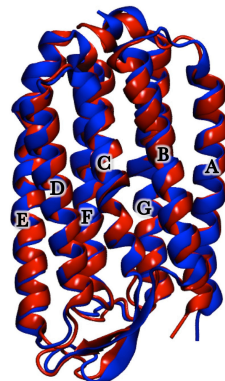


Figure S1. Overlay of the TM α -helices of the QM/MM optimized geometry (red) with the X-ray structure (blue).

II. Sequence Alignment

The sequence alignment shown in Figure S2 gives a visualization of the similarities between shR and related microbial rhodopsins. Clustal W⁴ was used to construct the sequence alignment between bacteriorhoropin (bR) (Uniprot ID: P02945), shR (Uniprot ID: P16102), and pharaonis halorhodopsin (phR) (Uniprot ID: P15647).



Figure S2. Comparative Sequence Alignment between bacteriorhodopsin (bR), and halorhodopsin from *halobacterium salinarum* (shR) and from *Natronobacterium pharaonis* (phR). Amino acids lining the seven transmembrane α -helices are highlighted in yellow and alignment corresponding to site R82, D85, D212 and K216 in bR are shown in black and red boxes.

III. The comparison of observed X-ray crystal structure (PDB: 1E12) and QM/MM optimized distances between key active site residues involving the chromophore, chloride ion, water molecules (2081, 2082, 2023) and residues S73, S76, R108, W112, S115.

Distances	X-ray (Å)	QM/MM (Å)
OD1 _{D238} ... N _{pSBT}	3.47	3.48
Cl ⁻ ... N _{pSBT}	3.76	3.33
Cl ⁻ ... NH1 _{R108}	7.12	5.95
Cl ⁻ ... O _{w2081}	3.13	3.10
Cl ⁻ ... O _{w2082}	4.84	3.34
Cl ⁻ ... O _{w2023}	3.21	3.11
Cl ⁻ ... O _{S115}	3.07	3.28
OD2 _{D238} ... O _{w2081}	2.76	2.62
OD2 _{D238} ... O _{w2082}	2.77	2.61
O _{w2082} ... NH1 _{R108}	2.80	2.88
O _{w2082} ... NE1 _{W112}	2.81	2.89
O _{w2023} ... O _{R108}	2.81	2.95
O _{w2023} ... OG _{S76}	2.66	2.69
O _{w2081} ... OG _{S73}	2.85	2.60

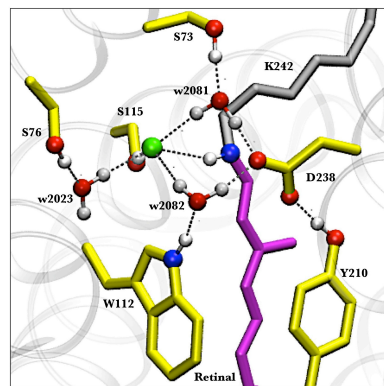


Figure S3. The active site of WT shR showing the protonated Schiff base of all-*trans*-retinyl chromophore (pSBT), two counterions (Cl⁻ in green and D238), active site waters (w2023, w2081 and w2082) and H-bond donor residues S73, S76, W112, S115 and Y210.

IV. Structural rearrangements due to H95 mutants.

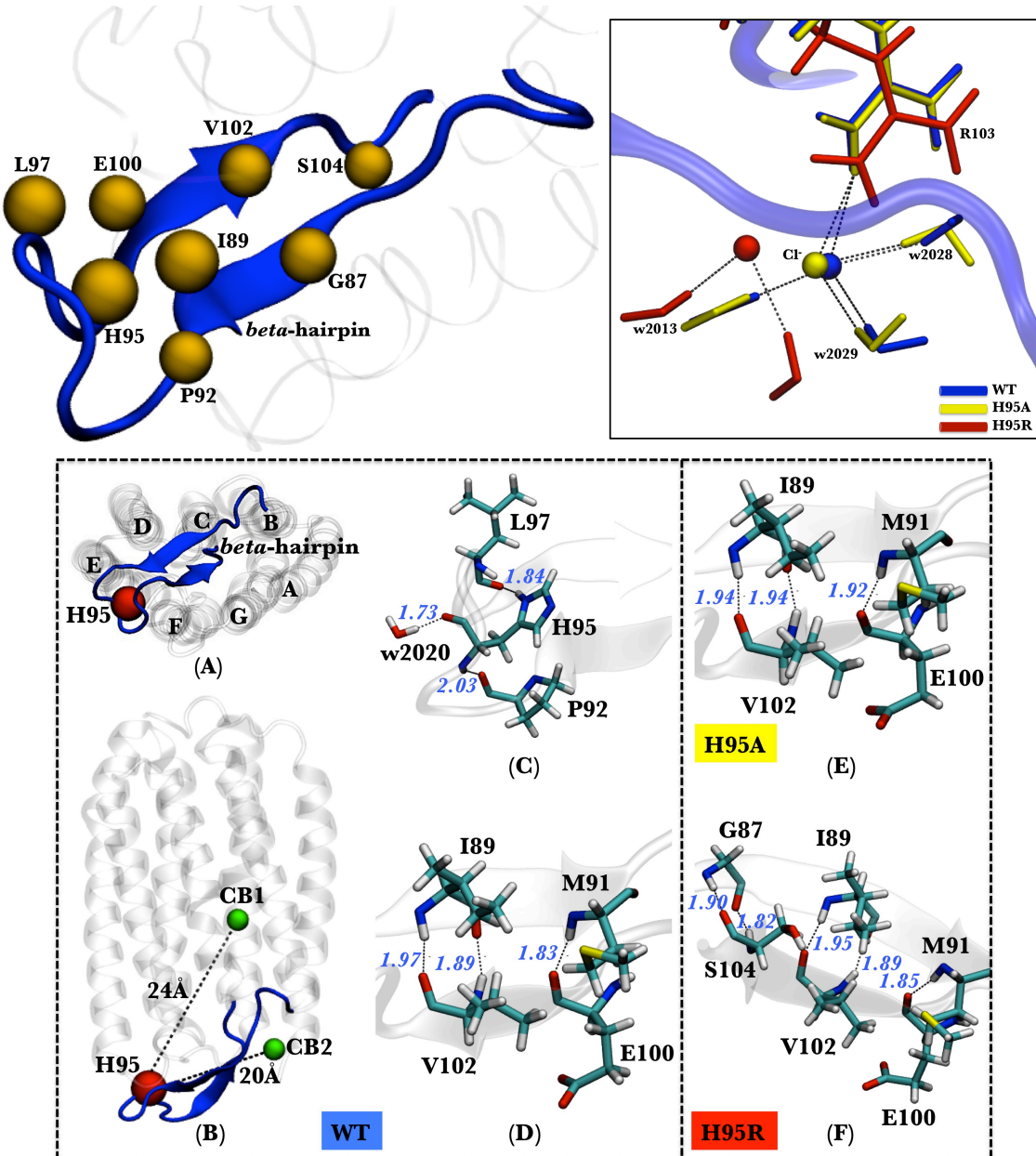


Figure S4: *Top panel left figure.* Location of site H95 at the center of the BC-loop spanning residues G87, I89, P92, L97, R100 and V102, respectively. These residues form crucial HBns within the loop. *Top panel right figure.* Structural perturbation of the salt bridge involving the CB2---R103 sites due to H95A (yellow) and H95R (red) mutants compared to the WT (blue). *Lower panel.* (A)-(B) Top- and lateral-views of site H95 and BC-loop situated between helices E, F and almost equidistant from sites CB1 and CB2. The HBns of (C)-(D) HBns around site H95 involving residues P92, L97 and 2020 and around the *beta*-hairpin region in the WT involving residues I89, V102, M91 and E100, (E)-(F) BC-loop of H95A being nearly identical to WT and (f) BC-loop of the H95R mutant involving residue G87, S104, I89, V102, M91 and E100.

V. Structural rearrangements due to Q105E, T111V and T203V mutants.

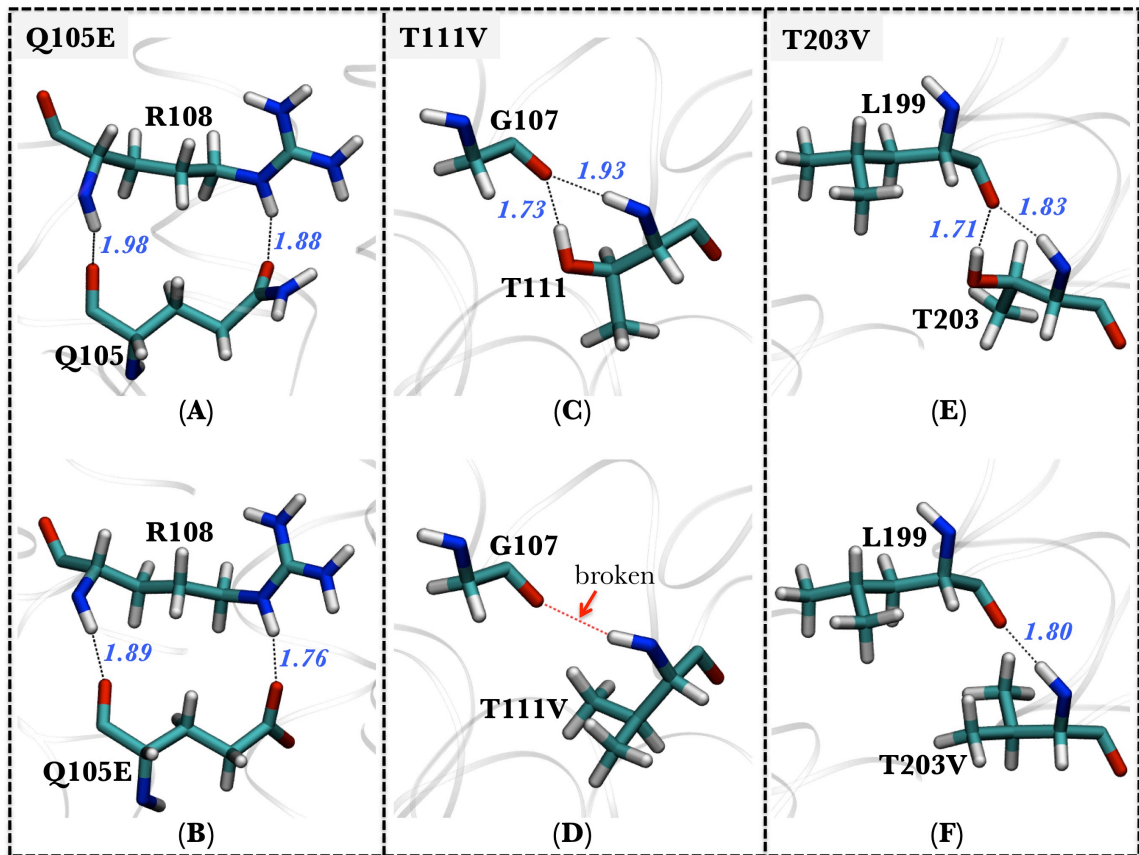
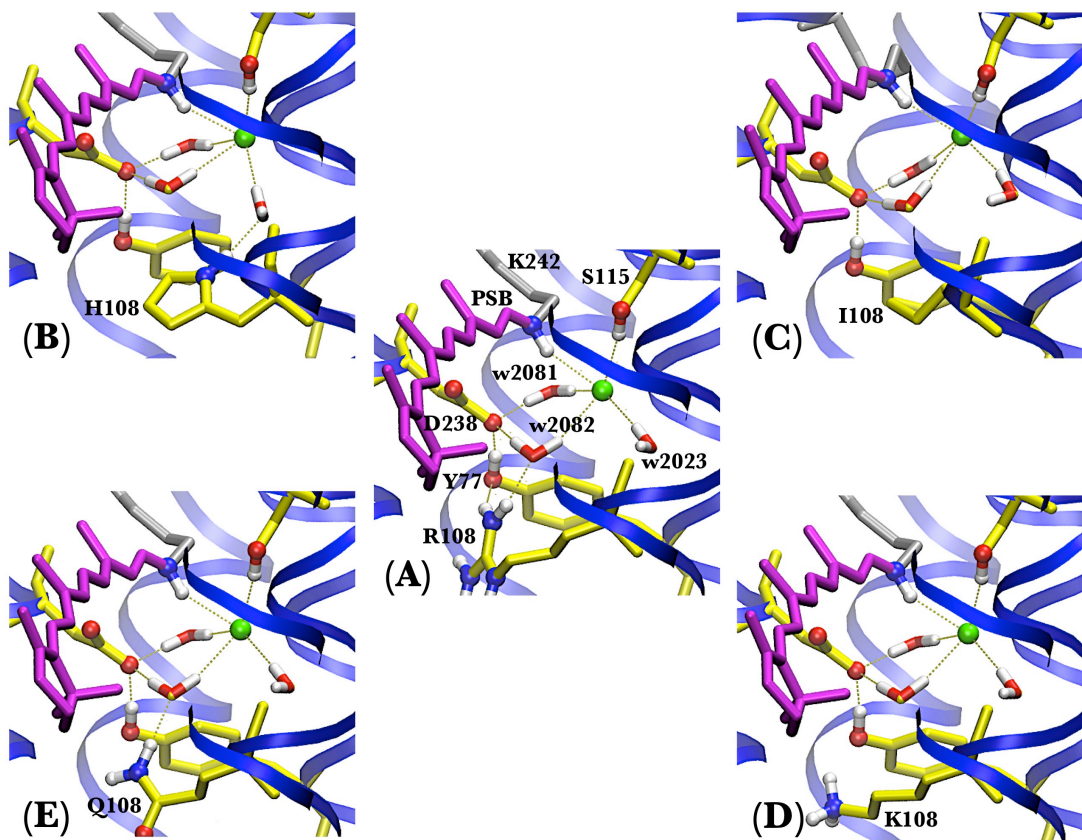
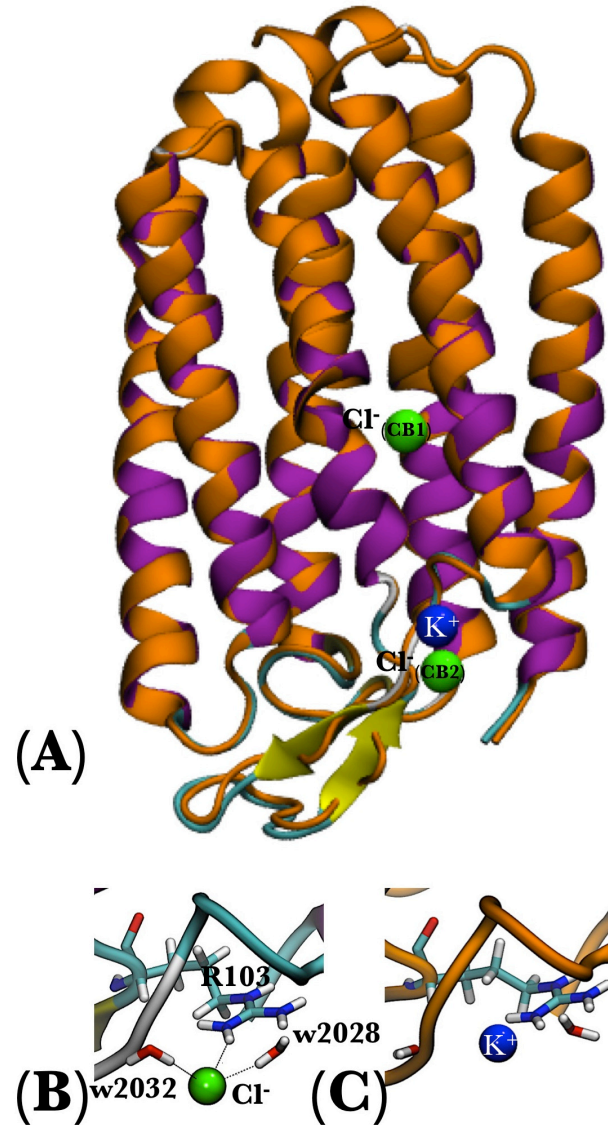


Figure S5. Residues Q105, T111 and T203 share two HBNs with R108, G107 and L199 via backbone and side chain atoms in the WT geometry. (A)-(B) In the presence of Q105E mutant, HB's between residues Q105 and R108 in the WT is shortened. (C)-(D) In the presence of T111V mutant, the two HB's between T111 and G107 is broken. (E)-(F) In the presence of T203V mutant, one of the two HB's between T203 and L199 is broken.

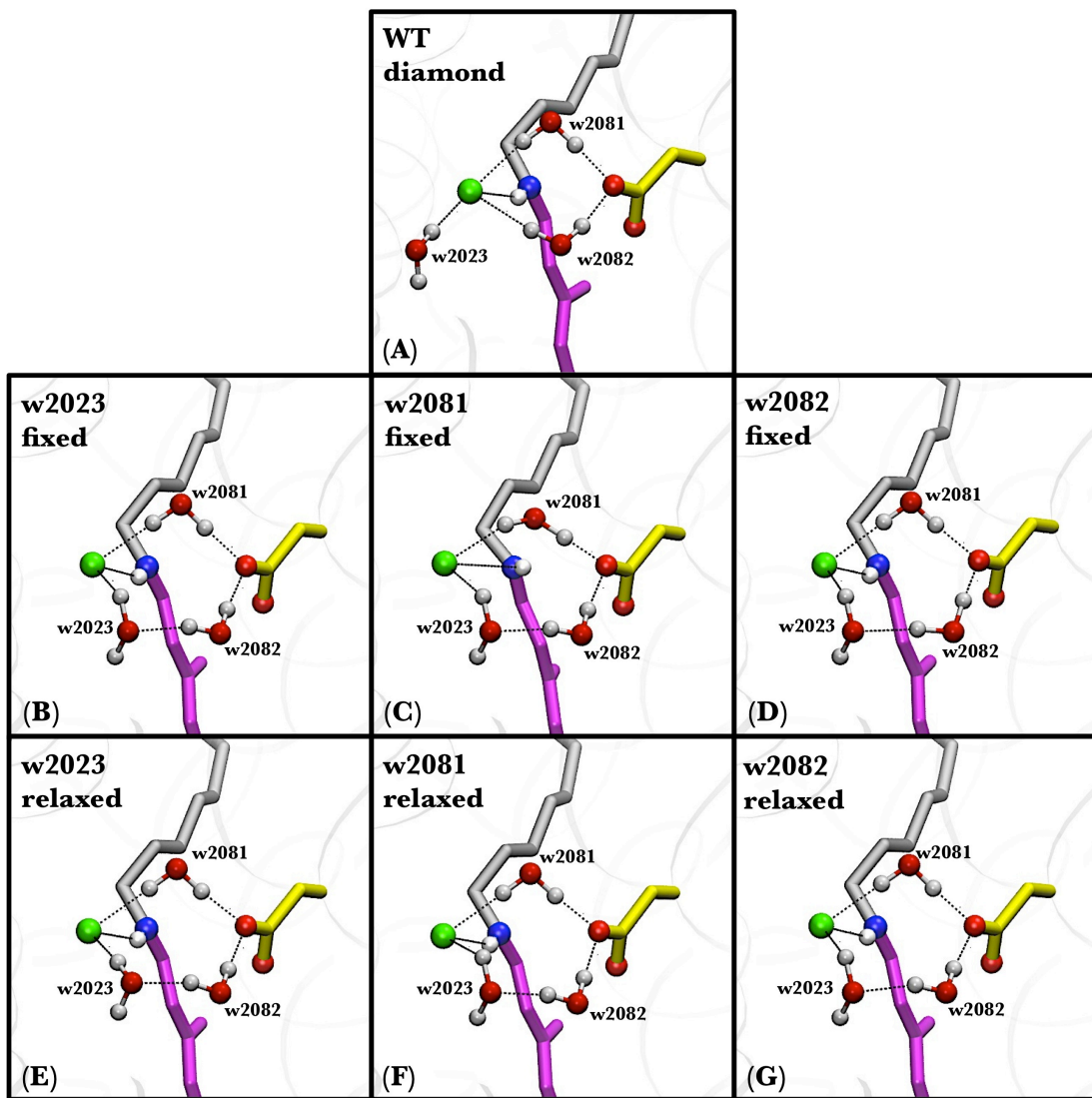
VI. The active site of the wildtype (**A**) and all the R108 mutants [R108H (**B**), R108I (**C**), R108K (**D**) and R108Q (**E**)] showing the hydrogen bonding of the R108 residue with the active site water molecule (w2082) is completely broken for all the mutants except for R108Q. R108H restores the broken hydrogen bond with w2082 by forming another bond with w2023. The interaction with Y77 and R108 NH₂ group is completely lost in all the mutants.



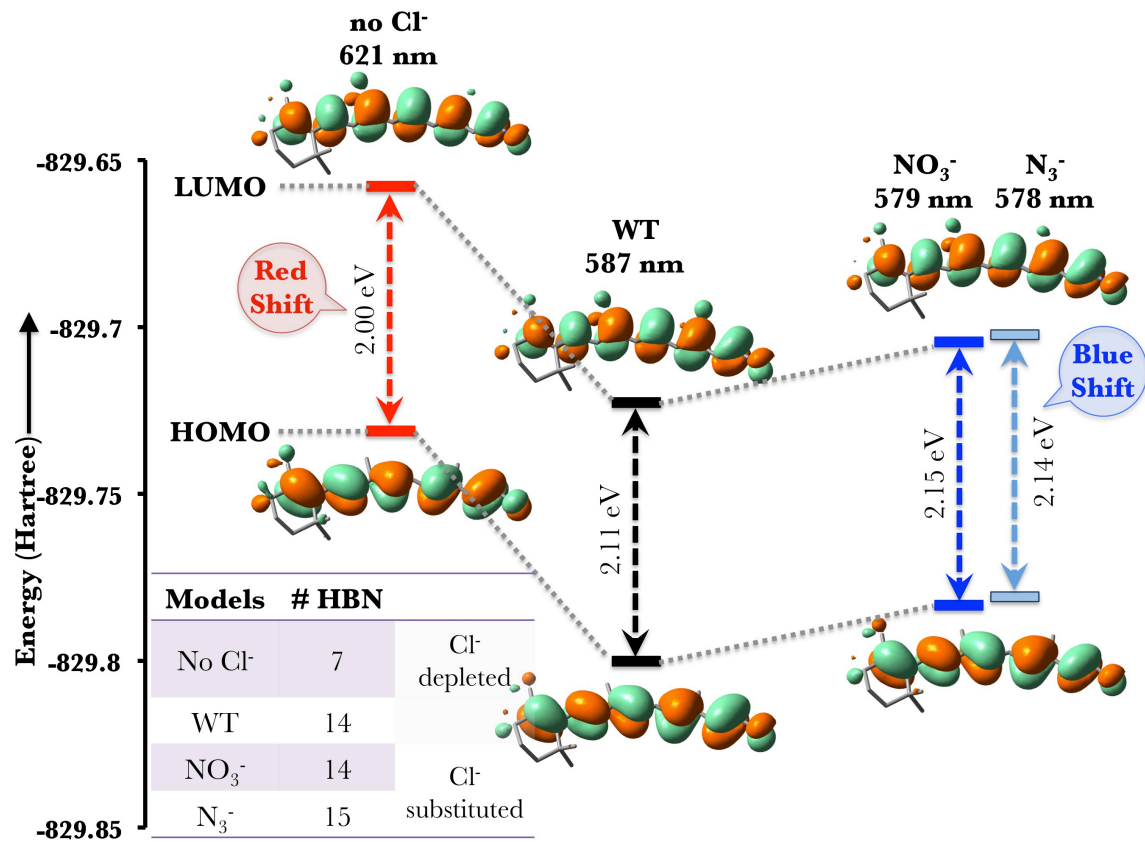
VII. **(A)** Overlay of the secondary structure of QM/MM optimized models of shR with Cl^- ions and with K^+ (orange color) in the CB2 site. **(B)** Presence of Cl^- at CB2 leads to the formation of hydrogen bonds between w2032, w2028, NH₂ group of R103. **(C)** In the presence of K^+ at CB2, no such hydrogen bonds are formed.



VIII. Comparison between the QM/MM optimized diamond-shaped water cluster and pentagonal water cluster in the active site. In order to mimic the pentagonal water cluster found in bR, we first fixed the position of w2023 in the WT optimized geometry (Fig. A) to its corresponding position in the X-ray structure and reoptimized the geometry (Fig. B). The resulting structure yields a pentagonal water cluster, which remained intact when the structure is relaxed without any constraints (Fig. E). We implemented the same procedure for the w2081 (Fig. C, F) and w2082 (Fig. D, G) sites, which also resulted in the formation of a pentagonal cluster in the active site of shR. However, the relative energies of the fully relaxed geometries (Fig. E, F, G) are high when compared to the WT geometry (Fig. A), which shows that the diamond shaped water cluster is more stable than the pentagonal water cluster. This property is attributed to the formation of an additional Cl---HOH bond in the diamond shaped water cluster. Therefore, we rule out the formation of a pentagonal water cluster in shR.



IX. Correlation between the total number of intermolecular hydrogen bonding networks in the active site and frontier molecular orbital analysis of the electronic transition responsible for the wavelength of maximal absorption in *s*HR.



The analysis shows that compared to the WT, decrease in the total number of HBN's in the active site due to Cl⁻ depletion decreases the energy gap between HOMO and LUMO and induces a spectral red shift. In contrast, increase in the total number of HBN's due to Cl⁻ substitution by N₃⁻ and NO₃⁻ increases the energy gap and induces a spectral blue shift.

X. The hydrogen bonding distances observed in the active site of wildtype shR and mutant (H95A, H95R, Q105E, R108K, R108I, R108Q, R108H, T111V, R200K, R200H, R200Q, R200A, T203V) models involving the chromophore, chloride ion, water molecules (2081, 2082, 2023) and residues S76, W112, S115, Y210, D238. Blue color represents bonds that are weakened and red color represents bonds that are broken compared to those in the wildtype.

HBN	Cl ⁻ ... H _{w2023}	Cl ⁻ ... H _{w2081}	Cl ⁻ ... H _{w2082}	Cl ⁻ ... H _{PSB}	Cl ⁻ ... OH _{S115}	OH _{S73} ... O _{w2081}	OD2 _{D238} ... H _{w2081}	OD2 _{D238} ... H _{w2082}	NH _{W112} ... O _{w2082}	OH _{S76} ... O _{w2023}	OD1 _{D238} ... OH _{Y210}
WT	2.13	2.13	2.39	2.39	2.31	1.62	1.64	1.65	1.89	1.71	1.58
H95A	2.13	2.14	2.36	2.39	2.31	1.62	1.64	1.65	1.88	1.71	1.58
H95R	2.12	2.13	2.33	2.40	2.28	1.61	1.63	1.64	1.89	1.72	1.57
Q105E	2.12	2.13	2.42	2.40	2.27	1.62	1.63	1.65	1.90	1.71	1.58
R108K	2.14	2.17	2.31	2.40	2.33	1.62	1.64	1.64	1.82	1.72	1.59
R108I	2.12	2.22	2.23	2.28	2.21	1.65	1.65	1.60	1.82	1.74	1.60
R108Q	2.14	2.17	2.36	2.59	2.29	1.63	1.64	1.64	1.86	1.72	1.58
R108H	2.14	2.24	2.25	2.37	2.23	1.61	1.61	1.61	1.86	1.71	1.59
T111V	2.13	2.14	2.38	2.35	2.31	1.62	1.63	1.65	1.87	1.68	1.58
R200K	2.13	2.13	2.36	2.40	2.28	1.62	1.64	1.65	1.89	1.71	1.57
R200H	2.12	2.14	2.36	2.37	2.30	1.62	1.64	1.65	1.88	1.70	1.58
R200Q	2.12	2.14	2.39	2.36	2.32	1.62	1.64	1.65	1.88	1.71	1.58
R200A	2.13	2.14	2.38	2.39	2.32	1.62	1.64	1.64	1.88	1.73	1.59
T203V	2.14	2.14	2.36	2.45	2.35	1.63	1.64	1.65	1.90	1.71	1.59
w/o Cl ⁻	---	---	---	---	---	1.76	1.59	1.65	1.93	1.90	1.61
D238p	2.14	2.06	2.19	2.31	---	1.83	1.85	2.81	1.90	1.72	---
NO ₃ ⁻	---	---	---	---	---	1.63	1.65	1.67	1.93	1.71	1.60
N ₃ ⁻	---	---	---	---	---	1.62	1.64	1.65	1.87	1.72	1.58
S115D	---	---	---	---	---	1.71	1.94	1.70	1.90	1.80	1.59
S115E	---	---	---	---	---	1.85	1.66	1.68	1.94	1.85	1.58

XI. SORCI+Q (6,6) calculated Vertical Excitation Energies in the gas phase and protein environments.

Table S1. The calculated SORCI+Q first vertical excited state absorption wavelengths (λ) in nm, oscillator (f) strengths in au and difference in the ground- (S_0) and excited state (S_1) dipole moments ($\Delta\mu$) of pSBT in gas-phase (QM-only) and in protein (QM/MM) environments of the wildtype and mutant models of halorhodopsin (shR). The corresponding experimental values are taken from references (5, 6 and 7) and the calculated spectral shift (experimental values in parentheses) between the wildtype and the mutants are also given.

shR	First Vertical Excited State ($S_1 \leftarrow S_0$) Properties						
	Gas phase		Protein			Expt.	Spectral Shift
	λ	f	λ	f	$\Delta\mu$		
Wildtype	636	1.77	587	1.85	15.2	578	-----
H95A	627	1.74	583	1.86	15.2	561	-4 (-17)
H95R	627	1.75	576	1.88	15.2	565	-11 (-13)
Q105E	634	1.76	581	1.81	15.0	560	-6 (-18)
R108H	631	1.72	562	1.87	15.0	565	-25 (-13)
R108I	617	1.79	548	1.85	14.7	563	-39 (-13)
R108K	637	1.72	577	1.85	15.0	565	-10 (-13)
R108Q	628	1.72	570	1.8	15.0	578	-17 (0)
T111V	631	1.80	577	1.82	15.0	575	-10 (-3)
R200A	627	1.74	580	1.86	15.1	572	-7 (-6)
R200H	634	1.75	580	1.88	15.2	578	-7 (0)
R200K	635	1.80	581	1.82	15.0	574	-6 (-4)
R200Q	626	1.74	580	1.85	15.1	579	-7 (+1)
T203V	637	1.73	588	1.79	14.9	580	+1 (+2)
NO_3^-	637	1.71	579	1.85	15.1	568	-8 (-10)
N_3^-	631	1.74	578	1.83	15.0	568	-9 (-10)
S115D	644	1.75	592	1.83	15.1	-	+5 (---)
S115E	626	1.78	585	1.87	15.4	-	-2 (---)
w/o Cl-	623	1.89	621	1.85	15.6	-	+34 (---)
w/o N_3^-	621	1.90	623	1.85	15.6	-	+36 (---)
w/o NO_3^-	641	1.73	625	1.83	15.6	-	+38 (---)
D238p	625	1.81	628	1.89	15.9	-	+41 (---)

XII. The dihedral angles (DA) along the all-*trans*-retinyl chromophore polyene chain in the QM/MM optimized wildtype and mutant (H95A, H95R, Q105E, R108K, R108I, R108Q, R108H, T111V, R200K, R200H, R200Q, R200A and T203V), without chloride, D238p, nitrate and azide model structures.

DA	C ⁵ -C ⁶ -C ⁷ -C ⁸	C ⁶ -C ⁷ -C ⁸ -C ⁹	C ⁷ -C ⁸ -C ⁹ -C ¹⁰	C ⁸ -C ⁹ -C ¹⁰ -C ¹¹	C ⁹ -C ¹⁰ -C ¹¹ -C ¹²	C ¹⁰ -C ¹¹ -C ¹² -C ¹³	C ¹¹ -C ¹² -C ¹³ -C ¹⁴	C ¹² -C ¹³ -C ¹⁴ -C ¹⁵	C ¹³ -C ¹⁴ -C ¹⁵ -N	C ¹⁴ -C ¹⁵ -N-C
WT	165.011	175.723	-176.065	175.087	-177.980	179.996	175.900	-169.111	177.934	-153.431
H95A	164.642	176.186	-177.364	174.956	-178.085	179.440	176.408	-170.044	178.766	-154.631
H95R	165.372	175.559	-177.344	174.929	-178.134	-179.959	175.817	-168.682	177.947	-152.225
Q105E	164.830	176.120	-177.541	174.627	-177.439	179.422	176.322	-169.467	177.964	-154.504
R108K	164.891	175.984	-177.113	174.835	-177.597	179.470	176.676	-169.805	178.569	-154.490
R108I	166.973	178.213	-176.923	178.172	-179.987	179.283	177.544	-176.593	176.196	-163.683
R108Q	166.532	176.630	-175.752	176.382	-176.138	-179.778	178.581	-165.815	176.800	-147.118
R108H	165.468	175.945	-176.833	175.904	-179.640	-179.045	174.012	-171.376	176.734	-160.052
T111V	165.105	175.840	-177.481	174.693	-177.760	179.368	176.209	-170.714	178.924	-154.367
R200K	165.557	175.811	-177.499	174.330	-177.600	179.378	176.160	-169.569	178.473	-153.089
R200H	164.666	176.340	-177.496	174.636	-177.841	179.389	176.404	-169.687	178.853	-153.134
R200Q	164.004	176.056	-176.899	174.731	-177.594	179.246	176.542	-170.292	178.894	-154.273
R200A	165.080	175.584	-176.849	174.977	-177.775	-179.953	176.000	-169.697	178.482	-154.612
T203V	165.983	176.447	-177.569	176.678	-178.111	-179.317	177.283	-168.445	177.641	-154.420
w/o Cl ⁻	166.242	176.302	-176.742	176.927	-178.340	-177.739	177.413	-162.257	179.786	-155.579
D238p	164.986	174.991	-178.807	174.766	-179.753	-179.676	174.394	-171.762	174.232	-159.795
NO ₃ ⁻	165.652	176.056	-177.179	177.966	-177.772	-178.753	179.144	-167.270	-179.260	-152.745
N ₃ ⁻	164.865	176.619	-176.706	177.245	-177.959	-179.041	177.696	-168.215	177.893	-159.217
S115D	164.595	174.839	-178.844	172.627	179.491	177.633	171.008	-178.306	170.979	-160.905
S115E	164.982	176.829	-179.201	174.171	-179.205	177.941	175.814	-174.888	179.731	-157.203

Bond lengths (BL) along the all-*trans*-retinyl chromophore polyene chain.

BL	C⁵-C⁶	C⁶-C⁷	C⁷-C⁸	C⁸-C⁹	C⁹-C¹⁰	C¹⁰-C¹¹	C¹¹-C¹²	C¹²-C¹³	C¹³-C¹⁴	C¹⁴-C¹⁵	C¹⁵-N
WT	1.373	1.455	1.368	1.437	1.387	1.407	1.386	1.406	1.406	1.378	1.339
H95A	1.374	1.455	1.367	1.437	1.387	1.407	1.386	1.406	1.406	1.378	1.339
H95R	1.372	1.455	1.366	1.437	1.386	1.408	1.385	1.406	1.405	1.379	1.340
Q105E	1.373	1.456	1.367	1.436	1.387	1.406	1.385	1.407	1.403	1.380	1.338
R108K	1.373	1.456	1.366	1.438	1.386	1.408	1.386	1.407	1.406	1.379	1.340
R108I	1.372	1.457	1.366	1.441	1.384	1.409	1.383	1.414	1.401	1.385	1.329
R108Q	1.372	1.456	1.367	1.439	1.386	1.408	1.384	1.408	1.402	1.382	1.335
R108H	1.371	1.458	1.366	1.439	1.385	1.410	1.383	1.410	1.402	1.382	1.335
T111V	1.373	1.455	1.367	1.438	1.388	1.407	1.387	1.406	1.404	1.379	1.338
R200K	1.374	1.454	1.366	1.437	1.387	1.407	1.387	1.406	1.405	1.379	1.339
R200H	1.374	1.455	1.368	1.437	1.387	1.407	1.386	1.406	1.406	1.378	1.341
R200Q	1.373	1.457	1.366	1.439	1.387	1.407	1.386	1.407	1.406	1.378	1.340
R200A	1.372	1.457	1.366	1.439	1.387	1.407	1.387	1.406	1.406	1.379	1.339
T203V	1.373	1.456	1.368	1.438	1.387	1.406	1.386	1.408	1.405	1.379	1.340
w/o Cl-	1.378	1.446	1.373	1.428	1.396	1.395	1.395	1.395	1.420	1.367	1.350
D238p	1.379	1.446	1.374	1.426	1.398	1.395	1.397	1.395	1.417	1.374	1.337
NO ₃ ⁻	1.374	1.456	1.367	1.438	1.385	1.408	1.385	1.408	1.404	1.380	1.337
N ₃ ⁻	1.373	1.457	1.366	1.438	1.386	1.408	1.384	1.408	1.404	1.380	1.337
S115D	1.372	1.454	1.366	1.435	1.386	1.405	1.385	1.404	1.407	1.373	1.355
S115E	1.372	1.455	1.366	1.437	1.388	1.407	1.386	1.406	1.405	1.380	1.338

Bond angles (BA) along the all-*trans*-retinyl chromophore polyene chain.

BA	C₅-C₆-C₇	C₆-C₇-C₈	C₇-C₈-C₉	C₈-C₉-C₁₀	C₉-C₁₀-C₁₁	C₁₀-C₁₁-C₁₂	C₁₁-C₁₂-C₁₃	C₁₂-C₁₃-C₁₄	C₁₃-C₁₄-C₁₅	C₁₄-C₁₅-C₁₆	C₁₅-N-C
WT	118.425	129.565	125.617	115.958	128.195	120.645	126.995	117.048	124.783	123.929	124.450
H95A	118.328	129.645	125.610	115.986	128.162	120.666	127.067	117.060	124.818	123.816	124.501
H95R	118.493	129.577	125.504	116.070	127.863	120.974	126.885	117.117	124.770	123.718	124.286
Q105E	118.232	129.693	125.287	116.022	127.918	120.692	126.998	116.975	124.908	123.637	124.667
R108K	118.477	129.545	125.670	115.942	128.302	120.535	127.229	116.999	124.890	123.711	124.421
R108I	118.352	130.220	125.094	116.979	126.299	124.051	124.266	119.483	122.703	126.056	122.606
R108Q	118.189	129.801	125.279	116.122	127.298	121.482	125.627	117.417	124.390	124.346	122.331
R108H	118.722	129.364	125.513	116.373	127.529	121.710	126.009	117.411	124.078	124.191	125.242
T111V	118.421	129.501	125.592	115.999	127.881	120.981	126.764	117.215	124.482	123.812	124.627
R200K	118.384	129.506	125.548	115.894	128.061	120.667	127.069	117.133	124.907	123.601	124.746
R200H	118.437	129.497	125.457	116.151	127.673	121.136	126.484	117.401	124.724	123.826	124.265
R200Q	118.386	129.594	125.432	116.193	127.752	121.165	126.470	117.386	124.577	124.054	124.349
R200A	118.571	129.501	125.915	115.822	128.281	120.576	127.106	117.306	124.740	123.699	124.522
T203V	118.368	129.731	125.663	115.951	128.357	120.694	126.571	117.040	125.651	123.698	123.876
w/o Cl-	117.875	129.329	125.446	115.720	127.725	120.828	126.853	117.311	124.983	125.091	123.620
D238p	117.999	129.280	125.536	115.714	128.150	120.677	127.198	117.593	125.032	124.355	126.738
NO ₃ ⁻	118.420	129.505	125.763	116.022	128.010	121.116	126.148	117.508	125.209	123.848	123.635
N ₃ ⁻	118.485	129.519	125.875	115.974	128.443	120.554	126.674	117.037	125.491	124.242	123.506
S115D	118.215	129.356	125.807	115.375	129.106	119.172	128.372	115.863	126.379	120.361	127.346
S115E	118.280	129.930	125.455	115.882	128.424	120.128	127.932	116.542	126.126	122.174	126.709

XIII. References for the Supporting Information

1. Kolbe, M.; Besir, H.; Essen, L.-O.; Oesterhelt, D. *Science* **2000**, 288, 1390.
2. Maestro v. 9.3 (Schrödinger, LLC, New York, NY, 2012).
3. Gemlin, W.; Zeth, K.; Efremov, R.; Heberle, J.; Tittor, J.; Oesterhelt, D. *Photochem. Photobiol.* **2007**, 83, 369.
4. Larkin, M. A. *et al.* Clustal W and Clustal X version 2.0. *Bioinformatics* **2007**, 23, 2947.

XIV. Complete references from the manuscript.

19. Frisch, M. J.; Trucks, G. W.; Schlegel, H. B.; Scuseria, G. E.; Robb, M. A.; Cheeseman, J. R.; Scalmani, G.; Barone, V.; Mennucci, B.; Petersson, G. A.; Nakatsuji, H.; Caricato, M.; Li, X.; Hratchian, H. P.; Izmaylov, A. F.; Bloino, J.; Zheng, G.; Sonnenberg, J. L.; Hada, M.; Ehara, M.; Toyota, K.; Fukuda, R.; Hasegawa, J.; Ishida, M.; Nakajima, T.; Honda, Y.; Kitao, O.; Nakai, H.; Vreven, T.; Montgomery, Jr., J. A.; Peralta, J. E.; Ogliaro, F.; Bearpark, M.; Heyd, J. J.; Brothers, E.; Kudin, K. N.; Staroverov, V. N.; Kobayashi, R.; Normand, J.; Raghavachari, K.; Rendell, A.; Burant, J. C.; Iyengar, S. S.; Tomasi, J.; Cossi, M.; Rega, N.; Millam, J. M.; Klene, M.; Knox, J. E.; Cross, J. B.; Bakken, V.; Adamo, C.; Jaramillo, J.; Gomperts, R.; Stratmann, R. E.; Yazyev, O.; Austin, A. J.; Cammi, R.; Pomelli, C.; Ochterski, J. W.; Martin, R. L.; Morokuma, K.; Zakrzewski, V. G.; Voth, G. A.; Salvador, P.; Dannenberg, J. J.; Dapprich, S.; Daniels, A. D.; Farkas, Ö.; Foresman, J. B.; Ortiz, J. V.; Cioslowski, J.; Fox, D. J. Gaussian, Inc., Wallingford CT, 2009.